Image analysis method for the measurement of water saturation in a two-dimensional experimental flow tank

Benjamin Belfort, Sylvain Weill, François Lehmann

Image analysis method for the measurement of water saturation in a two-dimensional experimental flow tank

Benjamin BELFORT[†,*], Sylvain WEILL[†] and François LEHMANN[†]

[†] *Université de Strasbourg, CNRS, ENGEES, LHyGeS UMR 7517, F-67000 Strasbourg, France*

Submitted to Journal of Hydrology

* Corresponding author
Laboratoire d'Hydrologie et de Géochimie de Strasbourg
Université Louis Pasteur - CNRS - UMR 7517
1 rue Blessig, 67084 Strasbourg, France

Tél : 33 368 850 386
Fax : 33 388 370 497
Mail : belfort@unistra.fr

Abstract

A novel, non-invasive imaging technique is proposed that determines 2D maps of water content in unsaturated porous media. This method directly relates digitally measured intensities to the water content of the porous medium. This method requires the classical image analysis steps, i.e., normalization, filtering, background subtraction, scaling and calibration. The main advantages of this approach are that no calibration experiment is needed, because calibration curve relating water content and reflected light intensities is established during the main monitoring phase of each experiment and that no tracer or dye is injected into the flow tank. The procedure enables effective processing of a large number of photographs and thus produces 2D water content maps at high temporal resolution. A drainage / imbibition experiment in a 2D flow tank with inner dimensions of 40 cm x 14 cm x 6 cm (L x W x D) is carried out to validate the methodology. The accuracy of the proposed approach is assessed using a statistical framework to perform an error analysis and numerical simulations with a state-of-the-art computational code that solves the Richards' equation. Comparison of the cumulative mass leaving and entering the flow tank and water content maps produced by the photographic measurement technique and the numerical simulations demonstrate the efficiency and high accuracy of the proposed method for investigating vadose zone flow processes. Finally, the photometric procedure has been developed expressly for its extension to heterogeneous media. Other processes may be investigated through different laboratory experiments which will serve as benchmark for numerical codes validation.

1. INTRODUCTION

Due to its location at the interface between the atmosphere, vegetation and the land surface, the vadose zone plays a crucial role in the hydrological cycle; it supports many processes controlling the complex relationships between precipitation, infiltration, surface runoff, evapotranspiration and groundwater recharge (Corwin *et al.*, 2006; Harter and Hopmans, 2004; Selker e*t al.*, 1999). Regarding the complex interactions involved, water content is a key variable that needs to be accurately measured and modelled in order to characterize the processes occurring in the unsaturated part of the soil, accounting for physical, chemical, hydrological and biological properties of the soil. Many existing studies aim to investigate the remaining challenges regarding these processes and their possible impacts on water resources management from agricultural, geotechnical, biogeochemical, hydrological or environmental perspectives. These challenges may involve the way to integrate data and models in soil modelling, the quantification of their uncertainty, the development of new validation datasets and multi-model approaches (Seneviratne et al., 2010; Vereecken et al., 2016).

Laboratory or small-scale field experiments are well suited to investigate the interconnected processes that occur in the vadose zone and lead to improved understanding through measurements. Several experimental setups including variably saturated flow conditions have been designed to investigate issues such as water table recharge and, the effects of capillary fringes, heterogeneity and anisotropy at the bench scale (e.g., Abdul and Gillham, 1989; Stauffer and Dracos, 1986; Stephens and Heermann, 1988; Tidwell and Glass, 1994; Vauclin *et al.*, 1979; Wildenschild and Jensen, 1999; Yeh and Harvey, 1990) or at the field scale (e.g., Hills *et al.*, 1991; Wierenga *et al.*, 1991). Although outside the scope of this paper, which focuses on the vadose zone, previous laboratory experiments investigating variable density groundwater flow (Konz *et al.*, 2008 - 2009a – 2009b; Schincariol and

Schwartz, 1990; Simmons *et al.*, 2002) or contaminant hydrogeological processes that involve, for instance, nonaqueous phase liquid (NAPL) flow behaviour in porous media (Chevalier and Petersen, 1999; Kamaruddin *et al.*, 2011; Kechavarzi *et al.*, 2000; Kechavarzi *et al.*, 2005; McNeil *et al.*, 2006; Oostrom *et al.*, 2003; Oostrom *et al.*, 2007; van Geel and Sykes, 1994) are worth mentioning, as they can provide inspiration in term of experimental design and monitoring solutions. All these experiments allow for direct investigation of the physical processes of concern and also produce datasets that are valuable for calibrating and validating numerical models.

Numerical models for vadose zone modelling have received increasing attention in the last several decades. Numerous efforts have been carried out to develop reliable tools in order to improve our understanding of flow and transport processes through physically based simulations and to improve our prediction capacities (e.g., Feddes *et al.*, 1988; Šimůnek and Bradford, 2008; van Genuchten *et al.*, 2014). The issue of validating these numerical models is of particular importance for the modelling community. Validation aims at verifying that the numerical results are in agreement with the physics of the problem being examined and that the mathematical and numerical approaches chosen during the development step are appropriate. Modellers often perform analytical, numerical or experimental benchmarking problems and carry out inter-comparisons (for instance, Noh *et al.*, 2015; Vanderborght *et al.*, 2005). Nonetheless, the development of benchmarks for subsurface computational geosciences remains a challenge because of the restricted access to the underground and difficulties in the characterization of porous media (see Caers, 2013). Experimental studies in the field, for example those carried out at the Las Cruces trench site (see Hills *et al.*, 1991; Wierenga *et al.*, 1991) can be used as a basis for the definition of numerical reference test cases and thus for validation (Diersch and Perrochet, 1999; Forsyth and Kropinski, 1997; Forsyth and Wu, 1995; Kirkland *et al.*, 1992; Younes *et al.*, 2013). In a practical sense, due to

the limited number of real world test cases available for validation, many computational codes are only validated through synthetically designed numerical test cases (e.g., Celia *et al.*, 1990), demonstrating the need for new reference experimental systems.

Although of primary importance for the direct understanding of processes and for the validation of numerical models, the measurement of water content remains complex, even under controlled conditions. Direct observation of processes occurring in porous media is generally not practicable. Thus, experimental systems are very often characterized through indirect measurements and/or direct measurements at only a few locations. Consequently, the measurement of water content has received particular attention in the scientific community (Dobriyal *et al.*, 2012; Ochsner *et al.*, 2013; Robinson *et al.*, 2008; Romano, 2014; Susha Lekshmi, 2014; Vereecken *et al.*, 2008), which aims to propose more accurate measurement techniques, to widen their spatial coverage and thus improve the quality of experimental studies.

In this context, non-invasive imaging techniques represent the most promising approach. These techniques have thus been extensively developed, especially for applications in contaminant hydrogeology research regarding multiphase flow processes involving NAPL (Kamaruddin *et al.*, 2011; Oostrom *et al.*, 2007; Werth *et al.*, 2010). The review by Oostrom *et al.* (2007) discusses different flow experiments and their associated qualitative / quantitative monitoring devices. Of the various imaging techniques, they focused particularly on (i) photon – attenuation - based methods, such as the gamma radiation method and the X-ray attenuation method, and (ii) photographic methods, such as the light reflection method (LRM), the light transmission method (LTM) and the multispectral image analysis method (MIAM). Quantitative light transmission visualization techniques have been applied to complex systems of transient flow fields containing contaminants, for example (e.g., Conrad *et al.*, 2002; Darnault *et al.*, 1998; Darnault *et al.*, 2001; Flores *et al.*, 2007; Glass *et al.*, 2000;

Niemet and Selker, 2001). Note that LTM is mainly used in micromodel experiments with narrow flow tanks and that UV light is often preferred (Bob *et al.*, 2008; Catania *et al.*, 2008; Corapcioglu *et al.*, 1997; Detwiler *et al.*, 2000; Huang *et al.*, 2002; Jones and Smith, 2005; Theodoropoulou *et al.*, 2003). Since it can be conducted with non-transparent porous media and wide flow tanks, image analysis based on reflected light has been largely used for intermediate scale experiments (e.g., Goswami and Clement, 2007; Konz *et al.*, 2008 - 2009a and 2009b; McNeil *et al.*, 2006; Oostrom *et al.*, 1992a and 1992b; Rahman *et al.*, 2005; Schincariol *et al.*, 1990; Schincariol *et al.*, 1993; Simmons *et al.*, 2002; Swartz and Schwartz, 1998; Van Geel and Sykes, 1994; Wildenschild and Jensen, 1999). Nonetheless, image noise, fluctuations in brightness and reflections from the surroundings can disturb the reflection intensity measurements. Kechavarzi *et al.* (2000) proposed the MIAM method, which consists of taking pictures at different wavelengths and developing relationships between the optical density of the reflectance and the NAPL, as well as the water saturation of sand samples. Hence, this method allows for the measurement of the degree of saturation of two fluids in a three-phase system (Flores *et al.*, 2011; Kechavarzi *et al.*, 2005; Kechavarzi *et al.*, 2008). Note that tracers or dye are generally added to improve the visualization of processes using imaging techniques. For instance, Schincariol *et al.* (1990) used Rhodamine WT liquid in their experiment on salt water plumes, Konz *et al.* (2008; 2009a) used Cochineal Red A (E124), whereas Darnault et al. (1998) coloured the water phase with 0.005% FD&C blue #1 in their soil-oil-water experimental setup.

The use of non-invasive imaging techniques to study unsaturated flow processes specifically is less common. The light transmission method (LTM) for the measurement of water content in unsaturated porous media was first described by Hoa (1981), who considered the relationship between the emergent light intensity passing through a sand sample and the number of pores that were full of water. A photosensitive surface collects the transmitted light

and the measured electrical resistance is related to the degree of illumination. A calibration procedure is then necessary to determine a linear relationship between water content and illumination. In the two-dimensional thin-slab system used by Tidwell and Glass (1994), the transmitted light intensity is recorded by means of digital imaging equipment. Hence, this saturation measurement technique is limited as suitable image contrast and nonopaque medium are required. Yoshimoto *et al.* (2011) directly measured the degree of saturation of an unsaturated porous medium using a bright red food dye and the light reflection method by relating variations in the colour of the medium with the water content changes.

Note that, in all optical measurement techniques, image processing is required to convert the reflected or transmitted light intensities into the variable of interest (i.e., saturation, concentration, …). This procedure generally consists of data conversion, selection of a sensitive channel, correction of brightness values for the LRM, and definition of a calibration curve. Although most lab-scale flow studies employ monochromatic grey-scale imaging, such treatments exploit only part of the available information. Nonetheless, quantification of colour differences, which is an essential step in obtaining results, can be very complicated because there are various ways to specify colour. For instance, colour can be specified in terms of a vector with three components that correspond to red, green and blue intensities (RGB), or using a system that includes hue, saturation and brightness components (HSB). It appears that no standard image processing exists in the literature and that the colour space selected for the analysis strongly impact the results (e.g., Kashuk *et al.*, 2014). For instance, the image analysis procedure used by Schincariol *et al.* (1993) is based on grey-scale values, as are those of Conrad *et al.* (2002) and Bob *et al.* (2008). On the other hand, Van Geel and Sykes (1994) used black and white images. Yoshimoto *et al.* (2011) proposed a quadratic relationship between water saturation and RGB luminance values. Darnault *et al.* (1998) suggested using the hue value of the transmitted light, which would be directly related

to the water content. Gerhard and Kueper (2003) found that the best correlation with fluid saturation was obtained for the saturation component of the HSB system. Finally, according to Konz *et al.* (2009a) and McNeil *et al.* (2006), the green channel is the most sensitive for determining the concentration.

The aim of this paper is to propose a non-invasive measurement technique that is based on both the analysis of photographic images and direct measurements to characterize 2D fields of water content. Compared to the method proposed by Yoshimoto et al (2011), which is the closest to ours, our approach has the following advantages. i) A unique tank is used so that the calibration and the experiment are carried out simultaneously in the same flow chamber. ii) Pure water is injected without any tracer or dye. iii) A unique digital camera is needed to perform the shooting. Finally, iv) the final estimation of water content is performed using the relationship between reflected light intensity values and water content based on numerous calibration points chosen during a drainage / imbibition experiment. Note that the methodology is validated on a 2D flow tank (14 cm x 40 cm x 6 cm), that the image processing is different, and that different colour space components are tested. Moreover, the overall quality of the measurement method is assessed using numerical simulations.

The paper is structured as follows. Section 2 describes the experimental setup, i.e., the flow tank used, the devices installed for direct and indirect measurements, the porous medium used as fill and the reference drainage / imbibition experiment carried out. The image analysis procedure is presented in section 3, in which are also explained the statistical method used to estimate the error and the numerical approach implemented for the comparison. The results of the photometric procedure investigated through the drainage / imbibition experiment are then described in section 4 and a discussion is proposed. Finally, the last section presents the conclusions of this study. It is important to mention that this article will serve, for example, as a guideline methodology to establish benchmarking experiments in larger flow tanks with

unsaturated heterogeneous media subjected to other boundary conditions. In addition, all technical specifications for equipment, data and programs are available upon request from the first author of the present paper.

2. MATERIALS AND EXPERIMENT

2.1. The 2D flow tank

Our novel photographic measurement method, that will be described in the next section, is tested on a rectangular flow tank. The walls of the tank are fabricated using 1.5 cm-thick, transparent sheets of Plexiglas®, allowing visual observation of water content changes. The tank consists of a unique flow chamber with internal dimensions 40 cm x 14 cm x 6 cm (L x W x D). An overflow outlet, whose height can be adjusted, is connected to two valves placed at the bottom of the tank. A 3-litre bottle is placed on a digital balance. Since a closed circuit is formed between the overflow outlet, the bottle on the balance and the peristaltic pump, we can follow the amount of water leaving and entering the tank.

The digital balance has a weighing capacity of 34 kg and a readability of 0.1 g. The other equipment associated with the validation flow tank are a light device placed horizontally at the bottom front of the tank, an opaque black curtain that is arranged around the tank and the camera, and a Theta probe (see section 2.2) placed vertically in the middle of the tank surface, which monitors the water content. A schematic representation of the experimental setup is shown in Figure 1.

2.2. Instruments used to take direct measurements

During the water flow experiments, water content, temperature and cumulative outflow can be monitored. Water content is measured using a Theta probe, Type ML2x (Delta-T Devices Ltd.), which is based on medium impedance measurements (Gaskin and Miller, 1996). For a range of measurements between 0.05 and 0.6 $m^3.m^{-3}$, the accuracy reaches ± 0.01 $m^3.m^{-3}$. The soil probe consists of four inert metal electrodes that are 6 cm in length and are inserted into the porous media. Hence, the soil moisture sensor has to be installed vertically at the top of the flow chamber. The soil sampling volume indicated by the manufacturer consists of a cylinder 4 cm in diameter by 6 cm in length (that is approximately 75 cm^3) surrounding the central rod. The Theta probe was calibrated through 1D column experiments that used different sand/water mixtures prepared over the whole range of water content values (from 0 to θs with a step of 0.05).

2.3. Image acquisition

The images are recorded using a Nikon digital camera D80, which is placed at a distance of approximately 2 metres from the tank. All camera parameters (ISO100, shutter speed 1/6 s, aperture F11.0) are set manually. We selected large size images with dimensions of 3872 pixels high by 2592 pixels wide. Linear images are captured in the RAW format (.nef), and these images are unprocessed files containing data from the image sensor. The digital camera also stores the automatically non-linearly processed photographs as .jpg images. In a linear image, the value at every pixel is directly related to the amount of light, i.e., the number of photons, received at that location on the sensor during the exposure. Hence, the RAW data includes the output from each of the original RGB-sensitive pixels of the image sensor, after being read out by the array electronics and passing through an analogue-to-digital converter. It also means that no gamma correction has been applied.

Image acquisition has to take into account the requirements of image processing, including pixel-by-pixel intensity tracking at different times. Therefore, the acquisition device is kept as uniform as possible throughout the duration of the experiment. With this requirement in mind, our camera is placed on a fixed metal tripod and is controlled by a computer program (Nikon Camera Control-PRO 2.11.0), which is not modified during the entire experiment.

2.4. Porous media

In the paper, which is dedicated to the description of our photometric procedure, the tank is homogenously packed. The porous medium was composed of monodisperse quartz sand (reference K30, from Kaltenhouse, France) with an average size of d_{50} = 493 μm and a coefficient of uniformity C_u = 1.595. Using a system composed of a funnel and PVC tubes, the sand is poured into the flow chamber in layers of a few millimetres at a time. During filling, there is always more water than sand in the tank in order to avoid the trapping of air. We use a rod to ensure that the medium is well placed and tap it gently with a piece of PVC to produce the most uniform compaction possible.

2.5. Experiment carried out

A single drainage / imbibition cycle is performed to test the image analysis method. The different steps of the experiment are listed in Table 1. Prior to the monitoring of water content and the amount of water on the balance, two drainage – imbibition cycles were carried out in order to stabilize the porous media. At the beginning of the experiment, the fully saturated tank was kept in this initial condition for 30 minutes. The drainage was then begun according to Table 1.

3. METHODS

The photometric procedure for obtaining water content maps is described in the present section. In addition, details concerning the statistical analysis and the numerical modelling approach will be given to complete this section, which presents our methods.

3.1. Photometric procedure

A program has been developed to automatically process the images according to the various successive steps described below.

- Importing the images and extracting their information

  Images stored in the .nef format (12-bit RAW data) are converted to 16-bit .tiff images, which have 65536 intensity values per channel in the RGB colour space. It allows us to linearly distribute the 12-bit information gained from the camera linearly over 16 bits. Hence, the data are preserved and channels are displayed as close as possible to how they are stored in the file. The properties of each imported image are stored in output files, particularly their timestamps.

- Selection of the colour space

  Then, the images are converted into the RGB colour space. According to the desired treatment, the macro automatically recognizes either RGB or HSB image stacking. The selected channel is kept, and the image is converted to a 32-bit image because of the operations required in our image analysis procedures. The first image of the series, which corresponds to the fully saturated condition, is considered to be the background image. Notice that we have tested the standard RGB and the individual red, green, blue, hue, saturation, and brightness channels. Surprisingly, the green channel seems to be the most appropriate for our first drainage / imbibition experiment. This result for saturation is in

concordance with the selection proposed by Konz *et al.* (2008) for the measurement of concentrations in density driven flows.

- Optionally, a median filter can be used (McNeil *et al.*, 2006; Schincariol *et al.*, 1993). Note that this step can be desirable for small validation tanks for which the pixel size is highly reduced. We used a radius value of 5. After selecting the green channel and applying the median filter, we denote the intensity of the pixel located at position (x, y) on the picture taken at time t as $I(x, y, t)$.

- Normalisation of the pre-processed image (to get $I_{cor}(x, y, t)$)

  White paper strips with a width of 2 cm are placed along the side and bottom boundaries of the tank and a black paper strip is present at the top edge of the tank. The minimum and maximum intensity values ($I_{\min}(t)$ and $I_{\max}(t)$) are measured for each picture and allow us to normalize the picture according to the following equation:

$$I_{cor}(x, y, t) = \left[I(x, y, t) - I_{\min}(t) \right] / \left[I_{\max}(t) - I_{\min}(t) \right] \quad [1]$$

  This step is essential to correct for possible fluctuations in lighting, which can affect the brightness values during the experiment (see Konz *et al.*, 2008).

- Obtaining $I_{proc}(x, y, t)$ through background subtraction

  For each image, the program subtracts the value of the background intensity pixel by pixel to obtain the corrected intensity. That is:

$$I_{proc}(x, y, t) = I_{cor}(x, y, t) - I_{cor}(x, y, 0) \quad [2]$$

  From a physical point of view, this equation represents differences in colour due to changes in soil moisture from its saturated state. The use of 32-bit images prevents data loss during this mathematical operation.

- Obtaining $I_{proc,av}(t)$ through the insertion of a measurement zone

  A rectangular zone is inserted that corresponds to the projected soil sampling volume of the Theta probe sensor on the front pane; its physical dimensions, 4 cm x 6 cm, represent 338 pixels x 506 pixels on the picture. Average intensities are automatically computed and stored in the results output file.

- Obtaining $\theta_{img}(x,y,t)$ through image calibration

  To relate a given processed intensity value to a water content θ_{img}, the relationship between direct measurements of water content made using the Theta probe sensor and indirect measurements carried out by the photometric technique has to be constructed and its parameters fitted. This step is only achieved when all the images taken during the experiment had been treated using the steps described previously. The curve is constructed from selected images at selected times during the experiment and for different wetting conditions. Following Yoshimoto *et al.* (2001) and Konz *et al.* (2008), various functions have been tested, of which the linear relation turns out to be the most suitable:

$$\theta_{img}(x,y,t) = a + b \times I_{proc}(x,y,t) \qquad [3]$$

- Conversion of processed intensities to water contents

  The photometric procedure is completed by using Eq. [3] to convert the processed intensity of each pixel in water content. This step can be applied at selected times for which moisture maps are required.

3.2. Statistical method

The issue of error analysis in estimating soil water content from our photographic procedure is analysed in the present section. Following Haverkamp *et al.* (1984), we add a stochastic disturbance term, e, to the right hand side term of Eq.[3], such that its expected

value $E(e)$ is zero and its variance $E(e^2)$ is constant (hypothesis of homoscedasticity). Since the true values of water content and intensity are affected by this error, the estimated linear correlation is usually written as follows:

$$\hat{\theta} = \hat{a} + \hat{b} \times \hat{I} \quad [4]$$

where $\hat{a}$ and $\hat{b}$ are estimates of the unknowns *a* and *b*, respectively, such that $E(\hat{a}) = a$ and $E(\hat{b}) = b$ for an unbiased estimator. The parameters can be obtained directly from the regression analysis (see also Johnston and Dinardo, 1997; Vandervaere *et al.*, 1994):

$$\hat{b} = \frac{s(\hat{I}, \hat{\theta})}{s^2(\hat{I})} \quad [5]$$

$$\hat{a} = \overline{\hat{\theta}} - \hat{b}\,\overline{\hat{I}} \quad [6]$$

$$s^2(e) = \frac{1}{Nm-2}\sum_{i=1}^{Nm} e_i^{\,2} = \frac{Nm}{Nm-2}\left(s^2(\hat{\theta}) - \hat{b} \times s(\hat{I}, \hat{\theta})\right) \quad [7]$$

$$s^2(\hat{b}) = \frac{s^2(e)}{Nm \times s^2(\hat{I})} \quad [8]$$

$$s^2(\hat{a}) = s^2(\hat{b}) \times \overline{\hat{I}^2} \quad [9]$$

$$s(\hat{a}, \hat{b}) = -s^2(\hat{b}) \times \overline{\hat{I}} \quad [10]$$

$$r^2 \approx \frac{s^2(\hat{I}, \hat{\theta})}{s^2(\hat{I}) \times s^2(\hat{\theta})} \quad [11]$$

where *Nm* is the number of pairs $(\hat{I}, \hat{\theta})$ used for the correlation, $s^2(e)$ is the disturbance variance, $s^2(\hat{a})$ and $s^2(\hat{b})$ are the estimated variances of $\hat{a}$ and $\hat{b}$, respectively, $s(\hat{b}, \hat{a})$ is the estimated covariance between $\hat{a}$ and $\hat{b}$, and r^2 is the square of the correlation coefficient.

The error of the estimated water content is composed of a calibration component $s_{Cal}{}^2\left(\hat{\theta}\right)$ and an instrumental component $s_{Inst}{}^2\left(\hat{\theta}\right)$ and can be expressed as follows:

$$s^2\left(\hat{\theta}\right) = s_{Cal}{}^2\left(\hat{\theta}\right) + s_{Inst}{}^2\left(\hat{\theta}\right) \quad [12]$$

$$s_{Cal}{}^2\left(\hat{\theta}\right) = s^2\left(e\right) + s^2\left(\hat{a}\right) + \hat{I}^2 \times s^2\left(\hat{b}\right) + 2 \times \hat{I} \times s\left(\hat{a},\hat{b}\right) \quad [13]$$

$$s_{Inst}{}^2\left(\hat{\theta}\right) = \left[\hat{b}^2 - s^2\left(\hat{b}\right)\right] \times s^2\left(\hat{I}\right) \quad [14]$$

Finally, the 68 % confidence interval in the water content $\hat{\theta}$ estimated from the processed intensity $\hat{I}$ corresponds to:

$$\hat{\theta} - t_{0.16} \times s\left(\hat{\theta}\right) < \hat{\theta} < \hat{\theta} + t_{0.16} \times s\left(\hat{\theta}\right) \quad [15]$$

In Eq [15], $t_{0.16} \approx 1.0$ is given by the Student distribution with $\left(Nm-2\right)$ degrees of freedom for a confidence interval of 68 %.

3.3. Modelling approach

Our image analysis method provides moisture maps, which are an interesting extension of local sensor measurements; nonetheless, these maps can also be obtained through numerical modelling. The purpose of this part is to present the modelling approach. The comparison between image analysis results and numerical simulations is discussed in the next section. Variably saturated flow in porous media can be described using Richards' equation (RE, see Eq.[16]), assuming that air remains at atmospheric pressure and the flow velocity can be estimated using Darcy–Buckingham's law.

$$\frac{\partial \theta}{\partial t} + S_S S_W \frac{\partial h}{\partial t} + \nabla.\left(-K\left(h\right).\nabla H\right) = f \quad [16]$$

In the mixed form of RE given above, H [L] and h [L] are the hydraulic piezometric and pressure heads, respectively, such that $H = h + z$; z [L] is the depth, which is taken to be

positive upward; S_S [L^{-1}] is the specific storage; S_W [-] is the relative saturation of the aqueous phase $\left(S_w(h)=\theta(h)/\theta_s\right)$; $\theta(h)$ [L^3L^{-3}] and θ_s [L^3L^{-3}] are the actual and saturated water contents respectively, *K(h)* [LT^{-1}] is the hydraulic conductivity as a function of pressure head; and *f* [T^{-1}] is the source-sink term.

The model description is completed by relationships relating water content and hydraulic conductivity to pressure head. The standard van Genuchten (1980) model is used here for the pressure-saturation relationship:

$$S_e=\frac{\theta-\theta_r}{\theta_s-\theta_r}=\begin{cases}\dfrac{1}{\left(1+\left(\alpha|h|\right)^n\right)^{1-1/n}} & h<0\\ 1 & h\geq 0\end{cases} \qquad [17]$$

where θ_r is the residual water content [L^3L^{-3}], α is a parameter related to the mean pore size, and n is a parameter reflecting the uniformity of the pore size distribution. For the conductivity-saturation relationship, Mualem's model has been adopted leading to (van Genuchten, 1980):

$$K\left(S_e\right)=K_S\times K_r\left(h\right)=K_S\times S_e^{1/2}\left(1-\left[1-S_e^{n/n-1}\right]^{1-1/n}\right)^2 \qquad [18]$$

in which S_e is given by Eq. [17], K_S is the saturated conductivity, K_r is the relative conductivity and $n>1$. The porous medium described in section 2.4 has been characterized in previous experimental studies. In the present work, we select a few parameter sets obtained by inverse modelling to perform our simulations (see Beydoun and Lehmann, 2006). In addition to the hydraulic parameters characterizing the porous medium $\left(K_S,\theta_s,\theta_r,\alpha,n,S_S\right)$ presented in Table 2, numerical solution of the mathematical model (Eqs. [16],[17] and [18]) requires the definition of initial and boundary conditions (at the surface, bottom and lateral parts of the flow chamber) characterizing the problem studied. In terms of initial conditions, the fully

saturated condition is required for the calibration procedure. Impermeable boundary conditions are applied at the top and lateral limits whereas a varying pressure head that corresponds to the outlet overflow displacements is given at the bottom boundary of the flow domain. All details about the numerical methods can be found in previous research articles (Belfort et al., 2013; Fahs et al., 2009).

4. RESULTS AND DISCUSSION

The proposed photometric procedure (cf. section 3.1) is applied. Figure 2 depicts the evolution of intensities within the zone of water content measurement at the top of the tank. Images are taken every minute during the experiment except between 28800 s and 86520 s where the time interval between photographs corresponds to 1 h. We do not provide water content measurements since they follow the same trend than intensities. Hence, for the first drainage step, only a few amount of water leaves the flow chamber. The air entry pressure should be overpassed to initiate water displacement. Then, larger variations are observed when the overflow outlet is moved downward at location – 20 cm (from 3600 s), – 30 cm (from 7200 s), – 40 cm (14400 s), – 50 cm (21600 s). Between 21600 s and 86520 s, intensities continue to increase; water content at the top of the tank decreases due to water equilibration in the flow chamber. Notice that the 3th drainage step provides the larger colour variation. The imbibition phase begins from 86520 s. Nevertheless, it is necessary to wait for the last two steps (-10 cm at time 108000 s and 0 cm from 115200 s until 122300 s) so that the surface water content increases again resulting in a more conspicuous decrease in intensity. Figure 2 illustrates the importance of normalizing the intensities (i.e., by applying Eq.[1]) and the effects of the median filter. Raw intensities suffer from larger variations than normalized intensities. Besides, the median filter allows to smooth the signal and to improve the quality of data treatment. The orange squares depicted in Figure 2 correspond to the 13

points used for the construction of the calibration curve. As indicated in section 3.1, the selected points coincide with the end of the different steps before the overflow outlet is moved. In this way, hydrodynamic effects are avoided.

After subtracting the background, calibration curve can be constructed and the regression coefficients determined (see Table 3). Figure 3 corresponds to the calibration curve and the associated confidence interval, as explained in section 3.1. The construction of the calibration curve is based on selected pictures from the period before the overflow outlet moves (see the locations of the orange squares in Figure 2). The values of parameters and their errors are listed in Table 3. The error in the processed intensity, $s^2\left(\hat{I}\right)$ of Eq. [14], corresponds to the maximum error encountered at the calibration points. In addition to the confidence interval, error bars related to the processed intensities and water content values are presented in Figure 3. Two points among the 13 calibration values are outside the confidence region but their error bars overlap its boundary or are very close. These points correspond with phases of strong variations in water content and intensities. Finally, this result seems to confirm the feasibility of the proposed methodology and especially the choice of calibration points (at the end of each outlet overflow displacement).

The photometric procedure is applied to the zone (4 cm x 6 cm) corresponding to the sensor location. The absolute and relative errors over time are then calculated as follows:

$$\theta\text{-}AbsErr_{cum}(j) = \frac{\sum_{i=1}^{j}\left|\theta_{cal,i} - \theta_{mes,i}\right|}{\sum_{k=1}^{j\max}\theta_{mes,k}} \times 100 \qquad [19]$$

$$\theta\text{-}RelErr_{cum}(j) = \frac{\sum_{i=1}^{j}\left(\theta_{cal,i} - \theta_{mes,i}\right)}{\sum_{k=1}^{j\max}\theta_{mes,k}} \times 100 \qquad [20]$$

where j refers to the desired printing time (between 1 and jmax = 1156; total duration is 48 h), i corresponds to the different dates of the photographs (actually each minute and each hour between the 5^{th} and 6^{th} steps), θ_{mes} is the measured water content and θ_{cal} is the value obtained using the photometric procedure. Figure 4 depicts the absolute and relative cumulative errors in the flow tank during the drainage / imbibition experiment. The cumulative error remains relatively small and it appears that this procedure leads to an overestimation of the water content during drainage and an underestimation during imbibition. As it has been observed for the calibration curve, phases with strong variations of water content and intensities lead to larger error in estimating water content by means of the photometric procedure.

Even if a satisfactory correlation coefficient has been obtained for the linear calibration curve depicted in Figure 3, the validation of the image analysis method has also been investigated through the cumulated mass of water entering and leaving the flow tank. The mass of water at a given time $M_w(t)$ is expressed as follows:

$$M_w\left(t_i\right)=\left[\sum_{j=1}^{Nz}\left(\hat{\theta}_j\left(t_i\right)-\hat{\theta}_j\left(t_0\right)\right)\times\Delta_j\right]\times\Delta_e \qquad [21]$$

where Nz refers to the number of zones (i.e., the number of pixels representing the front side of the tank: N_{px}), Δ_j is the size of the j^{th} zone (i.e., the size of each pixel after scaling of the picture: Δ_{px}), and Δ_e is the thickness of the tank. Moreover, considering the linear nature of the calibration curve and the initially saturated condition of the flow tank, Eq. [21] can be simplified as follows:

$$M_w\left(t_i\right)=\left[\sum_{j=1}^{Npx}\hat{I}_{proc,j}\left(t_i\right)\right]\times\hat{b}\times\Delta_{px}\times\Delta_e \qquad [22]$$

According to the error computation proposed by Vandervaere *et al.* (1994) for water content variation, the total variance might be given by the following equations:

$$s^2\left(M_w\right)=s_{Cal}{}^2\left(M_w\right)+s_{Inst}{}^2\left(M_w\right) \qquad [23]$$

$$s_{Cal}{}^2\left(M_w\right)=\left[\sum_{j=1}^{Npx}\hat{I}_{proc,j}\left(t_i\right)\right]^2\times s^2\left(\hat{b}\right)\times\left(\Delta_{px}\times\Delta_e\right)^2 \quad [24]$$

$$s_{Inst}{}^2\left(M_w\right)=N_{px}\times\hat{b}^2\times s^2\left(\hat{I}\right)\times\left(\Delta_{px}\times\Delta_e\right)^2 \quad [25]$$

The previous equations are used to compute the cumulative mass from the photographs of the flow tank and to evaluate the confidence interval limits. These results could be compared to the measured cumulative mass shown in Figure 5. We observe that the photometric procedure provides a quite accurate representation of the mass measurements, partly because the calculation integrates all pixel values and therefore includes both the errors stemming from the 2D water content computation and the scaling to the 3D volume of the water. The mean absolute error is approximately 35 g, which is slightly more than 5 % of the maximum value of the cumulative mass. During the drainage phase, the photometric procedure underestimates the mass variation, whereas it overestimates the mass variation during imbibition. Nonetheless, we point out that the different steps are reproduced and the maximum value is reached.

Simulations of the experimental setup have been performed according to the description provided in section 3.3. A triangular mesh with 560 elements (each element has an area of approximately 1 cm^2) is used. The mass of water entering or leaving the flow tank is also given by Eq. [21] in which the surface of each triangular element is taken into account. Different set of hydrodynamic parameters (see Table 2) obtained by inverse modelling approach (see Beydoun and Lehmann, 2006) have been selected to show the sensibility of the numerical results compared to those of image analysis method. Notice that theses parameters have not been estimated with the measurements of the present experiment but are taken from previous work on the same porous medium. Hence, Figure 6 depicts the evolution of the cumulative mass for both the numerical simulations and the photometric procedure. It is interesting to note that small variations in the parameter values affect the numerical estimates

of the cumulative mass. In simulation 1, which is characterized by the smallest α value, the total mass of water leaving the tank is underestimated by over 100 g. The other sets of parameters lead to overestimation of around 70 g. In comparison, the photometric procedure has an error around 15 g. The absolute cumulative mass error is computed according to Eq. [26]. The time interval adopted in the simulations to print the results is 30 minutes; jmax refers to the number of printing times (i.e. 69 values) and $M_{cal,i}$ (respectively $M_{mes,i}$) is the amount of water leaving the tank obtained from numerical simulations or photometric procedure (respectively measured with mass balance).

$$M\text{-}AbsErr_{cum} = \frac{\sum_{i=1}^{j\max} \left| M_{cal,i} - M_{mes,i} \right|}{\sum_{i=1}^{j\max} M_{mes,k}} \times 100 \qquad [26]$$

This error reaches 26 %, 16 %, 11 % and 19 % for simulations 1 to 4 respectively. We get 7% for the absolute cumulative mass error with the photometric procedure. Actually, the results obtained with the proposed photometric procedure are satisfactory compared to those obtained with the numerical model. Note that the numerical results could have been improved by directly using the measurements of our experiment to better estimate the set of hydrodynamic parameters. However, this point is beyond the scope of our article. We also provide in Figure 7 the water content maps obtained through the photometric procedure and numerical modelling at different times during the drainage and imbibition phases. The images derived from the photographs are averaged for a grid size composed of 560 square elements. Figure 7 contains photographs of the flow chamber at three times during drainage and imbibition. Processed images, water content maps obtained with the photometric procedure and resulting from simulations 1 and 3 are also presented. Although quantitative comparisons between photometric procedure and simulations have been made previously (Figure 6) , Figure 7 illustrates the interest of the image analysis method. Irregularities in water content

maps clearly appear on photographs whereas simulations cannot easily reproduce such observations. Figure 7 also shows the good correspondence between the photographs and the water content maps. Finally, we can observe the impact of hydraulic parameters on the numerical results. The drainage of the flow chamber is slower with the first set of parameters than with the third one. Conversely, during the imbibition phase, water saturation level in the tank progresses faster with the first set of parameters.

Following Konz *et al.* (2008) rather than Schincariol *et al.* (1993), Swartz and Schwartz (1998) or McNeil *et al.* (2006), a direct relationship between the measured intensities and moisture contents has been successfully investigated taking into account the possible perturbations. Obviously, in our study, it is not necessary to use the γ-calibration method (Rahman *et al.*, 2005) or to convert the measured intensities into optical densities (McNeil *et al.*, 2006; Schincariol *et al.*, 1993). These methods are generally used to account for variations in lighting, exposure or film development. According to Konz *et al.* (2008), this is explained by the fact that neither analogue images, nor automatically non-linearly adjusted and compressed images, are taken.

Moreover, the developed procedure is intended to be efficiently applied to a large number of images with high temporal and spatial resolution without excessive computational cost. The procedure has been developed to allow its extension to heterogeneous media, especially layered soils. Nonetheless, it remains necessary to install at least one probe in each representative layer and to achieve significant variations in its water content in order to construct the calibration curves associated with each type of soil. For the precision of the method, it is important that each layer has the closest structure and compaction as its representative layer containing the probe. While the photometric procedure is exclusively dedicated to laboratory experiments, it offers an interesting perspective for the validation of numerical models. Indeed, in addition to taking into account heterogeneity, new experiments

such as rainfall simulation or runoff problem may be considered. This would make it possible to build benchmarks for unsaturated codes that would no longer be based solely on local measurements of pressure head or water content, but also on water content maps. New processes could also be investigated such as hydrodynamic effects or evaporation at the surface layer.

5. CONCLUDING REMARKS

The use of photographs in soil sciences has been developed in the past several decades largely in order to facilitate the visualization of physical process. In the present study, we present a photometric methodology, which enables effective representation of water content evolution over time. From an experimental point of view, the originality of the proposed method is based on the direct use of colour variations, which occur due to water movement in soil, to characterize the degree of saturation of soil (without any tracer). The procedure includes image conversion, normalization to reduce the impacts of lighting variations, selection of an optimal work colour space (the green channel), optional median filtering (radius = 5), background subtraction (corresponding to the saturated state), scaling and calibration. Hence, by applying a linear calibration relation, a water content value is assigned to each pixel of the picture. It is also important to notice that the calibration step is carried out at the same time that the experiment occurs. Only a few images are used to construct the calibration curve; they represent different stabilized states of flow in the porous medium. Nonetheless, the method is capable of treating a large number of images with a high-resolution.

The photographic procedure is validated on a drainage / imbibition experiment carried out using a rectangular flow tank with internal dimensions of 40 cm x 14 cm x 6 cm (L x W x D) which allows to realize 2D water displacement. This procedure has advantages

when compared with conventional procedures, which are generally able to measure water content only at specific locations in the soil. In addition, an important aspect to complete is the statistical analysis. A section is devoted to this point and allows us to quantify the error and the confidence intervals. It shows the pertinence of the proposed method mainly in the experimental context, which is generally affected by large uncertainty sources. Curves depicting the cumulative mass of water leaving and entering the flow tank are proposed for the photometric procedure and the numerical simulations using Richards' Equation. Comparisons with mass balance measurements show the efficiency of the proposed methodology and underline the sensitivity of the numerical results to the hydraulic parameters used. Water content maps are given to complete the overview of the method. Finally, even if other results have not been published in this article, the experimental setup has been reproduced. Measurements and calibration with the photometric procedure are in good agreement with published results; they are slightly different due to variations in the structure of the porous medium and environmental conditions, which underlines the importance of applying the methodology directly during the experiment.

Ongoing work is aimed at developing a larger experimental flow tank and testing the photometric procedure outlined in the present article. Pressure head measurements could be included to increase the selection of monitoring devices. Hence, the objective of proposing a benchmark inspired by Vauclin's experiment (Vauclin et al., 1979), but directed at the unsaturated part of the soil, will be possible and could create the possibility of improving the validation of mathematical models. Different experimental conditions, including simulated rain, or heterogeneous media, for example, might be investigated. Other potential areas for improvement involve parameter estimation using inverse methods for numerical modelling of the experiment. For the soil used in the experiment detailed here, hydraulic parameters have been derived from a previous study; however, we observe that the numerical results are not

optimal. Finally, to conclude the perspectives part, we notice that the photographs show that the behaviour of the porous media is subject to dynamic effects and gravity fingering. Investigations of these subjects could be carried out in the future through the photographic procedure.

Acknowledgements

The authors are grateful to Jérôme MUTTERER and Mathieu ERHARDT (CNRS UPR 2357 (IBMP), Strasbourg) for their significant contribution to the image analysis method. We thank the editor Corrado Corradini, the associate editor Renato Morbidelli and the four anonymous reviewers for their helpful comments that improved this paper. The study was partially financed by Strasbourg University and ENGEES; we acknowledge their scientific councils for their confidence.

References

Abdul, A.S., Gillham, R.W., 1989. Field studies of the effects of the capillary fringe on streamflow generation. J. Hydrol. 112(1-2), 1-18. doi:10.1016/0022-1694(89)90177-7

Belfort, B., Younes, A., Fahs, M., Lehmann, F., 2013. On equivalent hydraulic conductivity for oscillation–free solutions of Richard's equation. J. Hydrol. 505, 202-217. doi:10.1016/j.jhydrol.2013.09.047

Beydoun, H., Lehmann, F., 2006. Expériences de drainage et estimation de paramètres en milieu poreux non saturé. C. R. Geoscience 338, 180–187. doi:10.1016/j.crte.2005.12.004

Bob, M.M., Brooks, M.C., Mravik, S.C., Wood, A.L., 2008. A modified light transmission visualization method for DNAPL saturation measurements in 2-D models. Adv. Wat. Resour. 31(5), 727-742. doi:10.1016/j.advwatres.2008.01.016

Caers, J., 2013. A special issue on benchmark problems, data sets and methodologies for the computational geosciences. Computers Geosciences. 50, 1–3. doi: 10.1016/j.cageo.2012.11.001

Catania, F., Massabo, M., Valle, M., Bracco, G., Paladino, O., 2008. Assessment of quantitative imaging of contaminant distributions in porous media. Exp. Fluids. 44(1), 167-177. doi:10.1007/s00348-007-0388-x

Celia, M. A., Bouloutras, E.T., Zarba, R.L., 1990. A general mass-consservative numerical solution for the unsaturated flow equation. Water Resour. Res. 26:1483-1496.

Chevalier, L.R., Petersen, J., 1999. Literature review of 2-D laboratory experiments in NAPL flow, transport, and remediation. J. Soil Contam. 8(1), 149–167. doi: 10.1080/10588339991339289

Conrad, S.H., Glass, R.J., Peplinski, W.J., 2002. Bench-scale visualization of DNAPL remediation processes in analog heterogeneous aquifers: surfactant floods and in situ oxidation using permanganate. J. Contam. Hydrol. 58(1–2), 13–49. doi:10.1016/S0169-7722(02)00024-4

Corapcioglu, M.Y., Chowdhury, S., Roosevelt, S.E., 1997. Micromodel visualization and quantification of solute transport in porous media. Water Resour. Res. 33(11), 2547-2558. doi:10.1029/97WR02115

Corwin, D.L., Hopmans, J., de Rooij, G.H., 2006. From field-to landscape-scale vadose zone processes: scale issues, modeling, and monitoring. Vadose Zone J. 5, 129–139. doi:10.2136/vzj2006.0004

Darnault, C.J.G., Throop, J.A., DiCarlo, D.A., Rimmer, A., Steenhuis, T.S., Parlange, J.-Y., 1998. Visualization by light transmission of oil and water contents in transient two-phase flow fields. J. Contam. Hydrol. 31(3–4), 337–348. doi:10.1016/S0169-7722(97)00068-5

Darnault, C.J.G., DiCarlo, D.A., Bauters, T.W.J., Jacobson, A.R., Throop, J.A., Montemagno, C.D., Parlange, J.-Y., Steenhuis, T.S., 2001. Measurement of fluid contents by light transmission in transient three-phase oil-water-air systems in sand. Water Resour. Res. 37(7), 1859-1868. doi:10.1029/2000WR900380

Detwiler, R.L., Rajaram, H., Glass, R.J., 2000. Solute transport in variable-aperture fractures: An investigation of the relative importance of Taylor dispersion and macrodispersion. Water Resour. Res. 36(7), 1611-1625. doi:10.1029/2000WR900036

Diersch, H.-J.G., Perrochet, P., 1999. On the primary variable switching technique for simulating unsaturated-saturated flows. Adv. Wat. Resour. 23(3), 271-301. doi:10.1016/S0309-1708(98)00057-8

Dobriyal, P., Qureshi, A., Badola, R., Hussain, S.A., 2012. A review of the methods available for estimating soil moisture and its implications for water resource management. J. Hydrol. 458–459, 110–117. doi:10.1016/j.jhydrol.2012.06.021

Fahs, M., Younes, A., Lehmann, F., 2009. An easy and efficient combination of the Mixed Finite Element Method and the Method of Lines for the resolution of Richards' Equation. Environmental Modelling & Software. 24(9), 1122-1126. doi:10.1016/j.envsoft.2009.02.010

Feddes, R.A., Kabat, P., Van Bakel, P.J.T., Bronswijk, J.J.B., Halbertsma, J., 1988. Modelling soil water dynamics in the unsaturated zone — State of the art. J. Hydrol. 100(1-3), 69-111.

Flores, G., Katsumi, T., Kamon, M., 2007. Evaluation of LNAPL migration under fluctuating groundwater by image analysis. Ann. Disas. Prev. Res. Kyoto Univ. 50, 399-405.

Flores, G., Katsumi, T., Inui, T., Kamon, M., 2011. A simplified image analysis method to study LNAPL migration in porous media. Soils and Foundations. 51(5), 835-847. doi:10.3208/sandf.51.835

Forsyth, P.A., Wu, Y.S., Pruess, K., 1995. Robust numerical methods for saturated-unsaturated flow with dry initial conditions in heterogeneous media, Adv. Water Resour. 18, 25-38. doi:10.1016/0309-1708(95)00020-J

Forsyth, P.A., Kropinski, M.C., 1997. Monotonicity considerations for saturated-unsaturated subsurface flow. Siam J. Sci. Comput., 18, 1328-1354. doi:10.1137/S1064827594265824

Gaskin, G.J., Miller, J.D., 1996. Measurement of Soil Water Content Using a Simplified Impedance Measuring Technique. J . agric . Engng Res. 63(2), 153-160. doi:10.1006/jaer.1996.0017

Gerhard, J.I., Kueper, B.H., 2003. Capillary pressure characteristics necessary for simulating DNAPL infiltration, redistribution, and immobilization in saturated porous media. Water Resour. Res. 39(8), 1213. doi:10.1029/2002WR001490

Glass, R.J., Conrad, S.H., Peplinski, W., 2000. Gravity-destabilized nonwetting phase invasion in macroheterogeneous porous media: Experimental observations of invasion dynamics and scale analysis. Water Resour. Res. 36(11), 3121–3137. doi:10.1029/2000WR900152

Goswami, R., Clement, P., 2007. Laboratory-scale investigation of saltwater intrusion dynamics. Water Resour. Res. 43(4), W04418. doi:10.1029/2006WR005151.

Harter, T., Hopmans, J.W., 2004. Role of vadose zone flow processes in regional scale hydrology: Review, opportunities and challenges. Pages 179-208 in R. A. Feddes, G. H.

de Rooij, and J. C. van Dam, editors. International Symposium on Unsaturated Zone Modelling: Progress, Challenges and Applications. Kluwer, Wageningen (The Netherlands), 3-5 October 2004.

Haverkamp, R., Vauclin, M., Vachaud, G., 1984. Error analysis in estimating soil water content from neutron probe measurements: 1. Local standpoint. Soil science. 137(2), 78-90.

Hills, R.G., Wierenga, P.J., Hudson, D.B., Kirkland, M.R., 1991. The second Las Cruces experiment: Experimental results and twodimensional flow predictions. Water Resour. Res. 27(10), 2707-2718. doi:10.1029/91WR01538

Hoa, N.T., 1981. A new method allowing the measurement of rapid variations of the water content in sandy porous media. Water Resour. Res. 17(1), 41-48. doi:10.1029/WR017i001p00041

Huang, W., Smith, C.C., Lerner, D.N., Thornton, S.F., Oram, A., 2002. Physical modelling of solute transport in porous media: evaluation of an imaging technique using UV excited fluorescent dye. Water Res., 36(7), 1843-1853. doi:10.1016/S0043-1354(01)00393-1

Johnston, J., DiNardo, J., 1997. Econometric Methods. 4th Edition, McGraw-Hill, New York.

Jones, E.H., Smith, C.C., 2005. Non-equilibrium partitioning tracer transport in porous media: 2-D physical modelling and imaging using a partitioning fluorescent dye. Water Res., 39(20), 5099-5111. doi:10.1016/j.watres.2005.09.044

Kamaruddin, S.A., Sulaiman, W.N.A., Rahman, N.A., Zakaria, M.P., Mustaffar, M., Sa'ari, R., 2011. A review of laboratory and numerical simulations of hydrocarbons migrations in subsurface environments. Journal of Environmental Science and Technology. 4(3), 191-214. doi:10.3923/jest.2011.191.214

Kashuk, S., Mercurio, S.R., Iskander, M., 2014. Visualization of dyed NAPL concentration in transparent porous media using color space components. J. Contam. Hydrol. 162–163, 1-16. doi:10.1016/j.jconhyd.2014.04.001

Kechavarzi, C., Soga, K., Wiart, P., 2000. Multispectral image analysis method to determine dynamic fluid saturation distribution in two-dimensional three-fluid phase flow laboratory experiments. J. Contam. Hydrol. 46(3–4), 265–293. doi:10.1016/S0169-7722(00)00133-9

Kechavarzi, C., Soga, K., Illangasekare, T.H., 2005. Two-dimensional laboratory simulation of LNAPL infiltration and redistribution in the vadose zone. J. Contam. Hydrol. 76(3–4), 211–233. doi:10.1016/j.jconhyd.2004.09.001

Kechavarzi, C., Soga, K., Illangasekare, T.H., Nikolopoulos, P., 2008. Laboratory Study of Immiscible Contaminant Flow in Unsaturated Layered Sands. Vadose Zone J. 7(1), 1-9. doi:10.2136/vzj2006.0177

Kirkland, M.R., Hills, R.G., Wierenga, P.J., 1992. Algorithms for solving Richards' equation for variably saturated soils. Water Resour. Res. 28(8), 2049-2058. doi:10.1029/92WR00802

Konz, M., Ackerer, P., Meier, E., Huggenberger, P., Zechner, E., Gechter, D., 2008. On the measurement of solute concentrations in 2-D flow tank experiments. Hydrol. Earth Syst. Sci. 12(3), 727-738.

Konz, M., Ackerer, P., Huggenberger, P., 2009a. Comparison of light transmission and reflection techniques to determine concentrations in flow tank experiments. Exp Fluids, 47(1), 85–93. doi:10.1007/s00348-009-0639-0

Konz, M., Younes, A., Ackerer, P., Fahs, M., Huggenberger, P., Zechner, E., 2009b. Variable-density flow in heterogeneous porous media - Laboratory experiments and

numerical simulations. J. Contam. Hydrol. 108(3–4), 168–175. doi:10.1016/j.jconhyd.2009.07.005

McNeil, J.D., Oldenborger, G.A., Schincariol, R.A., 2006. Quantitative imaging of contaminant distributions in heterogeneous porous media laboratory experiments. J. Contam. Hydrol. 84(1–2), 36–54. doi:10.1016/j.jconhyd.2005.12.005

Niemet, M.R., Selker, J.S., 2001. A new method for quantification of liquid saturation in 2D translucent porous media systems using light transmission. Adv. Wat. Resour. 24(6), 651–666. doi:10.1016/S0309-1708(00)00045-2

Noh, S.J., AN, H., Kim, S., Kim, H., 2015. Simulation of soil moisture on a hillslope using multiple hydrologic models in comparison to field measurements. J. Hydrol. 523, 342–355. doi:10.1016/j.jhydrol.2015.01.047

Ochsner, T.E., Cosh, M.H., Cuenca, R.H., Dorigo, W.A., Draper, C.S., Hagimoto, Y., Kerr, Y.H., Njoku, E.G., Small, E.E., Zreda, M., 2013. State of the Art in Large-Scale Soil Moisture Monitoring. Soil Sci. Soc. Am. J. 77(6), 1888-1919. doi:10.2136/sssaj2013.03.0093

Oostrom, M., Hayworth, J.S., Dane, J.H., Güven, O., 1992a. Behavior of dense aqueous phase leachate plumes in homogeneous porous media. Water Resour. Res., 28(8), 2123-2134. doi:10.1029/92WR00711

Oostrom, M., Dane, J.H., Güven, O., Hayworth, J.S., 1992b. Experimental investigation of dense solute plumes in an unconfined aquifer model. Water Resour. Res., 28(9), 2315-2326. doi:10.1029/92WR01265

Oostrom, M., Hofstee, C., Lenhard, R.J., Wietsma, T.W., 2003. Flow behavior and residual saturation formation of liquid carbon tetrachloride in unsaturated heterogeneous porous media. J. Contam. Hydrol. 64, 93–112. doi:10.1016/S0169-7722(02)00107-9

Oostrom, M., Dane, J.H., Wietsma, T.W., 2007. A Review of Multidimensional, Multifluid, Intermediate-Scale Experiments: Flow Behavior, Saturation Imaging, and Tracer Detection and Quantification. Vadose Zone J. 6(3), 610-637. doi:10.2136/vzj2006.0178

Rahman, A., Jose S., Nowak W., Cirpka, O., 2005. Experiments on vertical transverse mixing in a large-scale heterogeneous model aquifer. J. Contam. Hydrol. 80(3-4), 130-148. doi: 10.1016/j.jconhyd.2005.06.010

Robinson, D. A., Campbell, C. S., Hopmans, J. W., Hornbuckle, B. K., Jones, S. B., Knight, R., Ogden, F., Selker, J., Wendroth, O., 2008. Soil Moisture Measurement for Ecological and Hydrological Watershed-Scale Observatories: A Review. Vadose Zone J. 7, 358–389. doi:10.2136/vzj2007.0143

Romano, N., 2014. Soil moisture at local scale: Measurements and simulations. J. Hydrol. 516, 6-20. doi:10.1016/j.jhydrol.2014.01.026

Schincariol, R.A., Schwartz, F.W., 1990. An experimental investigation of variable density flow and mixing in homogeneous and heterogeneousmedia. Water Resour. Res. 26(10), 2317–2329. doi:10.1029/WR026i010p02317

Schincariol, R.A., Herderick, E.E., Schwartz, F.W., 1993. On the application of image analysis to determine concentration distributions in laboratory experiments. J. Contam. Hydrol. 12(3), 197–215. doi:10.1016/0169-7722(93)90007-F

Selker, J.S., McCord, J.T., Keller, C.K., 1999. Vadose zone processes. Lewis Publishers, Boca Raton, FL.

Seneviratne, S.I., Corti, T., Davin, E.L., Hirschi, M., Jaeger, E.B., Lehner, I., Orlowsky, B., Teuling, A.J., 2010. Investigating soil moisture–climate interactions in a changing climate: a review. Earth-Sci. Rev. 99, 125–161. doi:10.1016/j.earscirev.2010.02.004

Simmons, C.T., Pierini, M.L., Hutson, J.L., 2002. Laboratory Investigation of Variable-Density Flow and Solute Transport in Unsaturated–Saturated Porous Media. Transp. Porous Media. 47(2), 215-244. doi:10.1023/A:1015568724369

Šimůnek, J., Bradford, S.A., 2008. Vadose Zone Modeling: Introduction and Importance.Vadose Zone J. 7, 581–586. doi:10.2136/vzj2008.0012

Stauffer, F., Dracos, T., 1986. Experimental and numerical study of water and solute infiltration in layered porous media. J. Hydrol. 84(1), 9-34. doi:10.1016/0022-1694(86)90042-9

Stephens, D.B., Heermann, S., 1988. Dependence of anisotropy on saturation in a stratified sand. Water Resour. Res. 24(5), 770-778. doi: 10.1029/WR024i005p00770

Susha Lekshmi, S.U., Singh, D.N., Shojaei Baghini, M., 2014. A critical review of soil moisture measurement. Measurement. 54, 92–105. doi:10.1016/j.measurement.2014.04.007

Swartz, C.H., Schwartz, F.W., 1998. An experimental study of mixing and instability development in variable-density systems. J. Contam. Hydrol., 34(3):169-189. doi: 10.1016/S0169-7722(98)00088-6

Theodoropoulou, M.A, Karoutsos, V., Kaspiris, C., Tsakiroglou, C.D., 2003. A new visualization technique for the study of solute dispersion in model porous media. J. Hydrol. 274(1–4), 176-197. doi:10.1016/S0022-1694(02)00421-3

Tidwell, V.C., Glass, R.J., 1994. X ray and visible light transmission for laboratory measurement of two-dimensional saturation fields in thin-slab systems. Water Resour. Res. 30(11), 2873-2882. doi:10.1029/94WR00953

Vanderborght, J., Kasteel, R., Herbst, M., Javaux, M., Thiéry, D., Vanclooster, M., Mouvet, C., Vereecken, H., 2005. A Set of Analytical Benchmarks to Test Numerical Models of Flow and Transport in Soils. Vadose Zone J. 4, 206-221. doi:10.2136/vzj2005.0206

Vandervaere, J.P., Vauclin, M., Haverkamp, R., 1994. Error analysis in estimating soil water balance of irrigated fields during the EFEDA experiment: 1. Local standpoint. J. Hydrol. 156(1–4), 351–370. doi:10.1016/0022-1694(94)90085-X

Van Geel, P.J., Sykes, J.F., 1994. Laboratory and model simulations of a LNAPL spill in a variably-saturated sand, 1. Laboratory experiment and image analysis techniques. J. Contam. Hydrol. 17(1), 1-25. doi:10.1016/0169-7722(94)90075-2

van Genuchten, M.T., Naveira-Cotta, C., Skaggs, T.H., Raoof, A., Pontedeiro, E.M., 2014. The use of numerical flow and transport models in environmental analyses, in Application of Soil Physics in Environmental Analyses: Measuring, Modelling and Data Integration, edited by W.G. Teixeira et al., pp. 349–376, Springer, Cham, Switzerland.

van Genuchten, M.Th., 1980. A closed-form equation for predicting the hydraulic conductivity of unsaturated soils. Soil Sci. Soc. Am. J. 44(5), 892–898. doi:10.2136/sssaj1980.03615995004400050002x

Vauclin, M., Khanji, D., Vachaud, G., 1979. Experimental and numerical study of a transient, two-dimensional unsaturated-saturated water table recharge problem. Water Resour. Res. 15(5), 1089–1101. doi:10.1029/WR015i005p01089

Vereecken, H., Huisman, J. A., Bogena, H., Vanderborght, J., Vrugt, J. A., Hopmans, J. W., 2008. On the value of soil moisture measurements in vadose zone hydrology: A review. Water Resour. Res. 44, W00D06. doi:10.1029/2008WR006829

Vereecken, H., Schnepf, A., Hopmans, J.W., Javaux, M., Or, D., Roose, T., Vanderborght, J., Young, M.H., Amelung, W., Aitkenhead, M., Allison, S.D., Assouline, S., Baveye, P., Berli, M., Brüggemann, N., Finke, P., Flury, M., Gaiser, T., Govers, G., Ghezzehei, T., Hallett, P., Hendricks Franssen, H.J., Heppell, J., Horn, R., Huisman, J.A., Jacques, D., Jonard, F., Kollet, S., Lafolie, F., Lamorski, K., Leitner, D., McBratney, A., Minasny, B., Montzka, C., Nowak, W., Pachepsky, Y., Padarian, J., Romano, N., Roth, K.,

Rothfuss, Y., Rowe, E.C., Schwen, A., Šimůnek, J., Tiktak, A., Van Dam, J., van der Zee, S.E.A.T.M., Vogel, H.J., Vrugt, J.A., Wöhling, T., Young, I.M., 2016. Modeling Soil Processes: Review, Key Challenges, and New Perspectives. Vadose Zone J. 5. doi:10.2136/vzj2015.09.0131

Werth, C.J., Zhang, C., Brusseau, M.L., Oostrom, M., 2010. A review of non-invasive imaging methods and applications in contaminant hydrogeology research. J. Contam. Hydrol. 113(1–4), 1–24. doi:10.1016/j.jconhyd.2010.01.001

Wierenga, P.J., Hills, R.G., Hudson, D.B., 1991. The Las Cruces trench site: Characterization, experimental results, and one-dimensional flow predictions. Water Resour. Res. 27(10), 2695-2705. doi:10.1029/91WR01537

Wildenschild, D., Jensen, K.H., 1999. Laboratory investigations of effective flow behavior in unsaturated heterogeneous sands. Water Resour. Res. 35(1), 17–27. doi:10.1029/98WR01958

Yeh, T.-C.J., Harvey, D.J., 1990. Effective unsaturated hydraulic conductivity of layered sands. Water Resour. Res. 26(6), 1271-1279. doi:10.1029/WR026i006p01271

Yoshimoto, N., Orense, R.P., Tanabe, F., Nikkawa, N., Hyodo, M., Nakata, Y., 2011. Measurement of degree of saturation on model ground by digital image processing. Soils and Foundations. 51(1), 167-177. doi:10.3208/sandf.51.167

Younes, A., Fahs, M., Belfort, B., 2013. Monotonicity of the cell-centred triangular MPFA method for saturated and unsaturated flow in heterogeneous porous media. Journal of Hydrology. 504, 132-141. doi:10.1016/j.jhydrol.2013.09.041

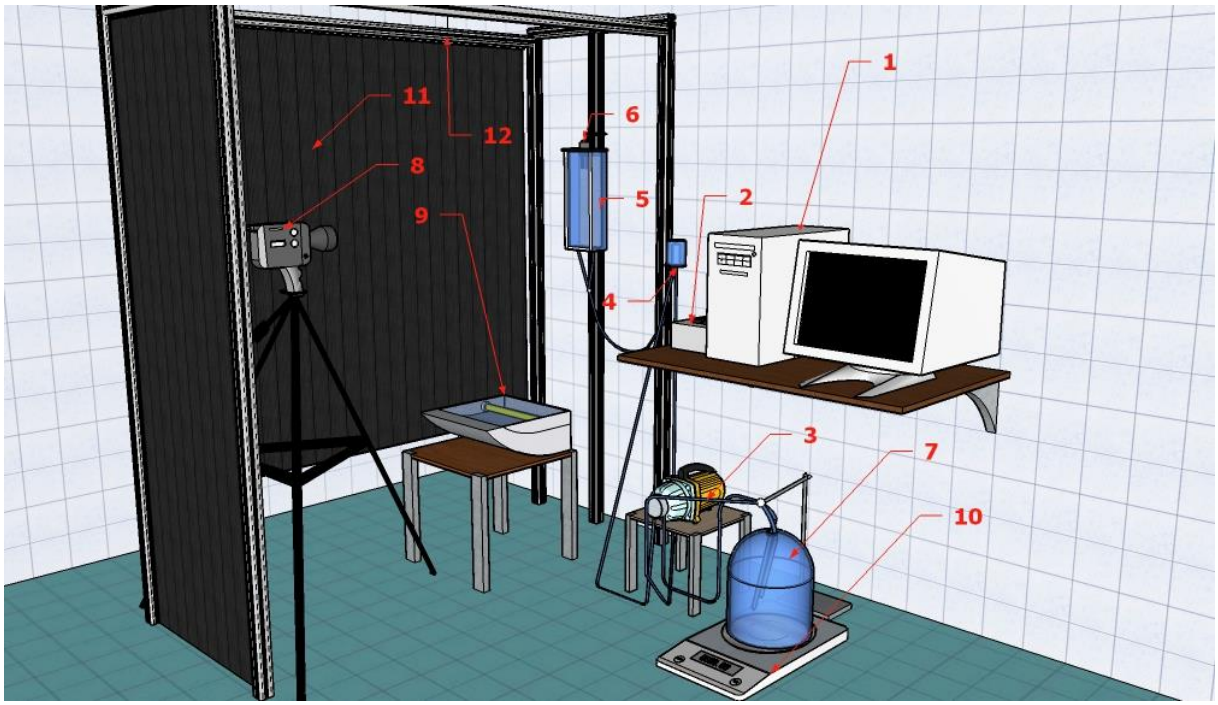

Figure 1 Schematic representation of the experimental setup (1: computer (softwares: Keysight VEE, ImageJ, Nikon Camera Control) – 2: data logger – 3: peristaltic Cole-Parmer pump – 4: overflow outlet (can be moved along the vertical axis) – 5: Plexiglas flow tank (40 cm x 14 cm x 6 cm) – 6: Theta probe ML2x – 7: bottle with pure water – 8: NIKON digital camera D80 – 9: floodlight (400 W) – 10: Sartorius digital balance – 11: black curtain (all around the experiment) – 12: Norcan metallic structure)

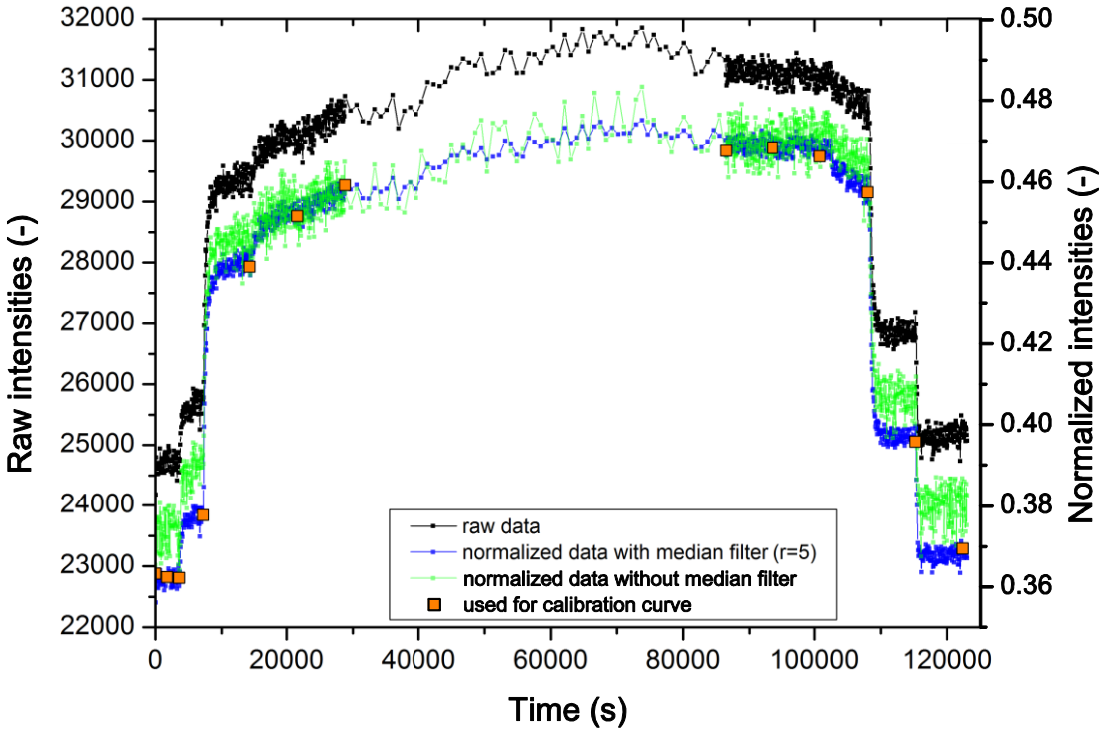

Figure 2 Evolution of the mean intensity corresponding to the water content zone of measurement; black curve and symbols depict raw data, blue (green respectively) curve and symbols represent the normalized data after median filter (without median filter respectively). Orange squares correspond to the values used for the calibration curve construction.

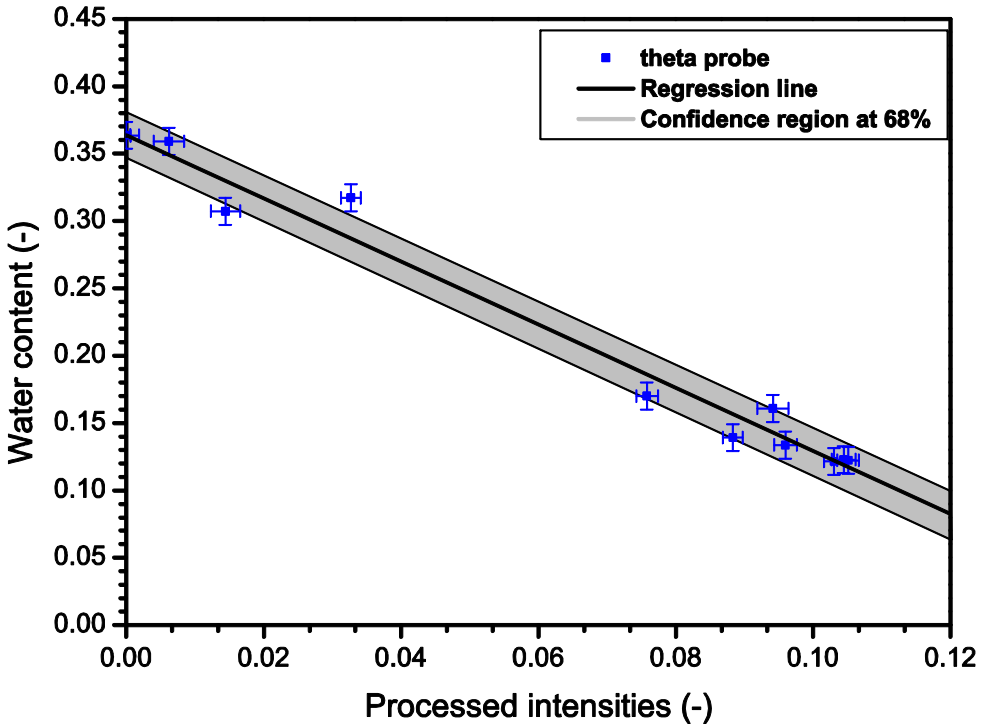

Figure 3 Intensity vs. water content calibration plot of the theta probe installed in the validation flow tank; regression line and confidence intervals at 68 %. The horizontal and vertical bars correspond to the maximal measurement error on estimated to one standard deviation.

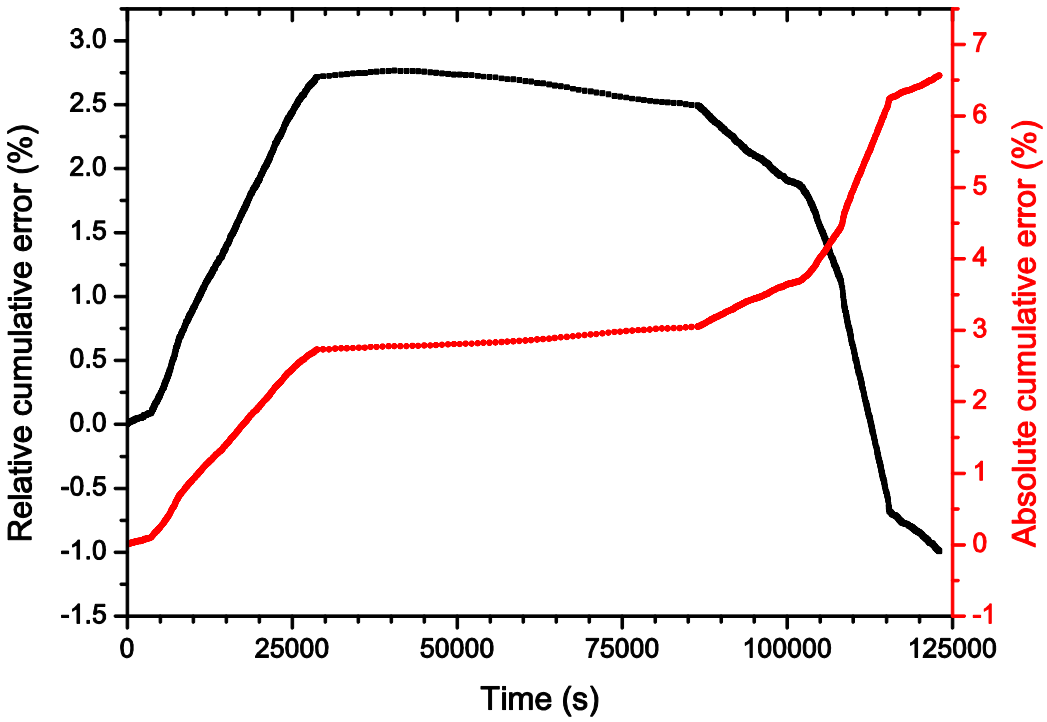

Figure 4 Evolution of the error on water content in the flow tank: absolute cumulative error (red solid line, computed with Eq.[20]) and relative cumulative error (black solid line, computed with Eq.[21]) between measurements and computation.

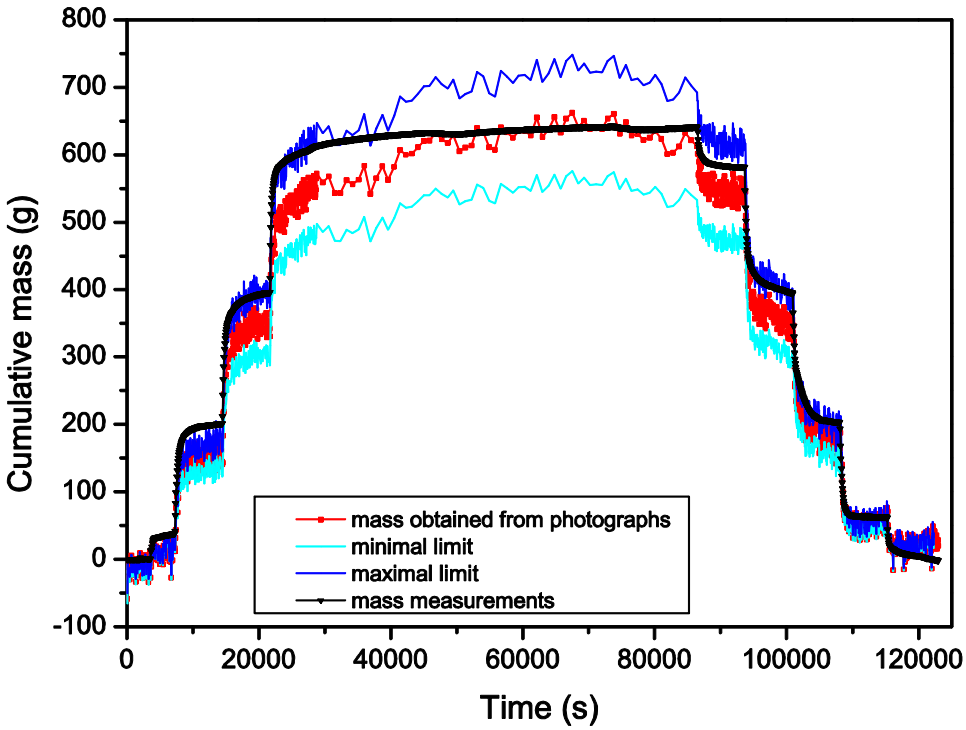

Figure 5 Evolution of the cumulative mass entering and leaving the flow tank.

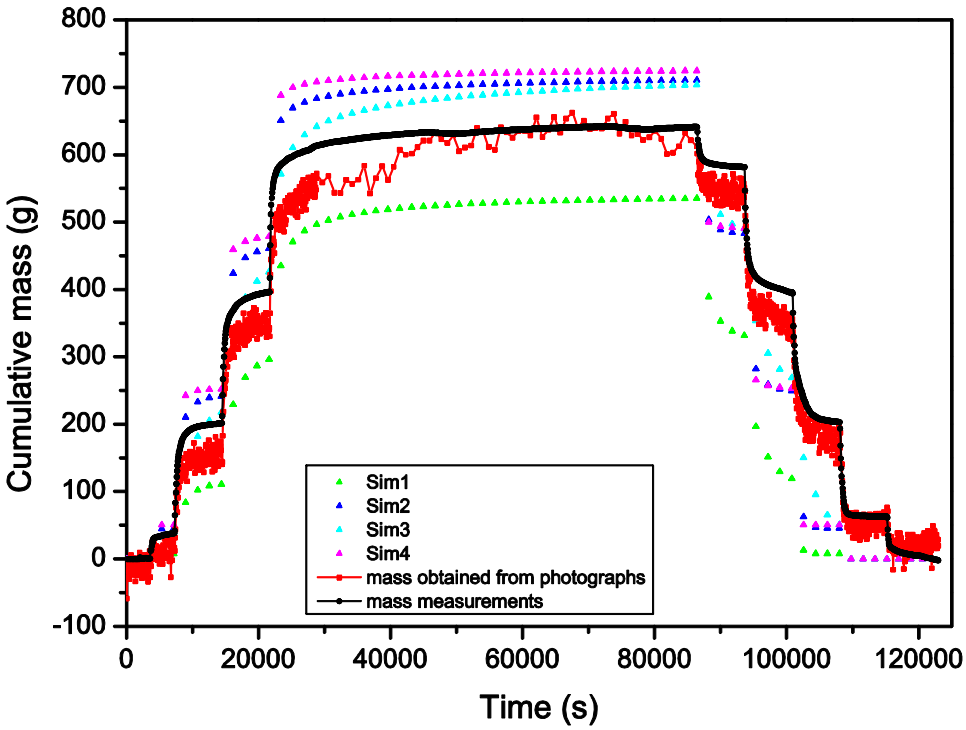

Figure 6 Cumulative mass of water entering and leaving the validation flow tank during drainage / imbibition experiment: comparison of measured values (black symbols and line), values of photometric procedure (red symbols and line) and results of modelling (coloured triangles).

Time and BC	Photographs	Processed Images	Maps from photometric procedure	Maps from numerical modelling Simul-1	Maps from numerical modelling Simul-3
7200 s End of the 2nd drainage step (-20cm)			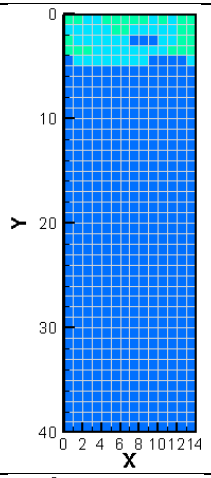	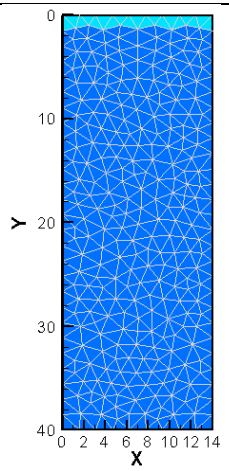	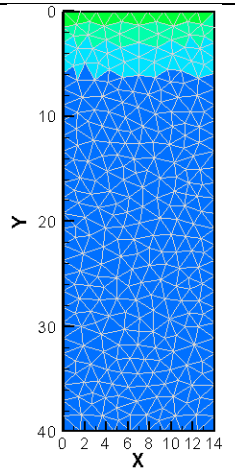
28800 s Final position for drainage step (-50cm)		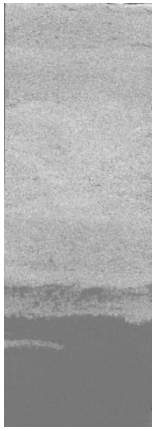	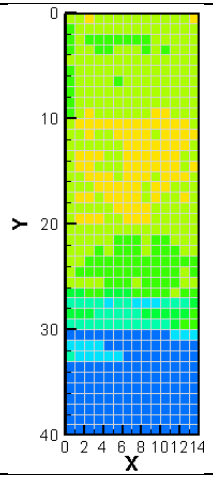	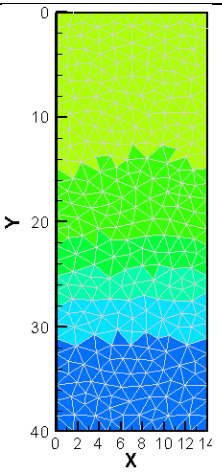	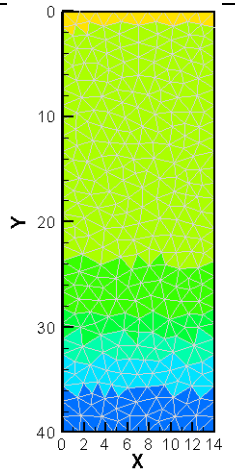

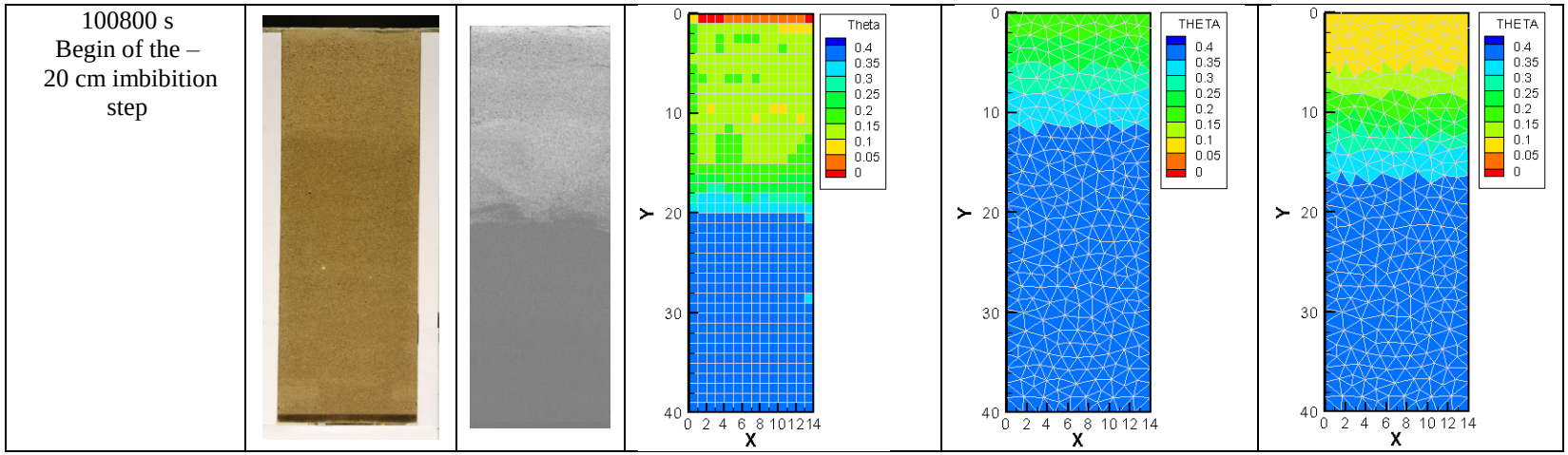

Figure 7 Illustrations of the proposed photometric procedure. Images before and after treatment. Comparison of water content maps obtained through photometric procedure and numerical modelling (simulation 1 and 3).

Table 1. Experimental procedure: movement of the overflow outlet responsible of transient flow in the flow chamber.

Step number	1	2	3	4	5	6	7	8	9	10
Overflow outlet displacement (cm)	-10	-10	-10	-10	-10	10	10	10	10	10
Step duration (h)	0.5	0.5	1	2	20	2	2	2	2	2
Elapsed time at the end of the step (h)	0.5	1	2	4	24	26	28	30	32	34

Table 2. Hydrodynamic parameters of Mualem van Genuchten used to simulate drainage / imbibition experiments.

parameters	K_s ($cm.s^{-1}$)	θ_s ($cm^3.cm^{-3}$)	θ_r ($cm^3.cm^{-3}$)	α (cm^{-1})	n (-)	S_s (cm^{-1})
Sim1	$5.0\ 10^{-3}$	0.375	0.099	0.04	7.45	$1\ 10^{-10}$
Sim2	$1.2\ 10^{-2}$	0.375	0.087	0.053	7.45	$1\ 10^{-10}$
Sim3	$3.76\ 10^{-3}$	0.372	0.076	0.052	7.39	$1\ 10^{-10}$
Sim4	$2.74\ 10^{-2}$	0.376	0.088	0.054	7.37	$1\ 10^{-10}$

Table 3. Calibration parameters and statistics of linear regression.

Parameter	Value	Standard Error
$\hat{a}$	0.3635	0.0066
$\hat{b}$	-2.3425	0.0934
r^2	0.98	
$s\left(\hat{a},\hat{b}\right)$	-0.0004	
$s^2(e)$	0.00022	0.01501
$s^2\left(\hat{I}\right)$	$5.2\ 10^{-6}$	0.002281